J Mater Sci (2010) 45:1709–1714
DOI 10.1007/s10853-009-3904-y

Amorphous Li–B–W–O solid-state electrolyte thin film for a solid-state ionic power sources

Seung Hyun Jee · Jun Young Oh · Ho Sang Ahn · Dong-Joo Kim · Howard C. Wikle III · Soo Ho Kim · Young Soo Yoon

Received: 1 July 2009 / Accepted: 15 September 2009 / Published online: 20 January 2010

Abstract Li–B–W–O thin film serving as a solid-state electrolyte layer for a solid-state thin film battery has been deposited on a stainless steel (SUS)/Si substrate by thermal evaporation deposition at room temperature. By energy dispersive X-ray spectroscopy and inductively coupled plasma-atomic emission spectrometer measurements, the as-grown thin film showed a stoichiometry of $Li_{2.99}BW_{1.8}O_9$. The as-grown Li–B–W–O solid-state electrolyte thin film possessed an amorphous structure as confirmed by X-ray diffraction. Field emission scanning electron microscopy measurements of the film cross section showed a dense structure that did not have any large defects such as cracks or voids. For a cell structure of SUS/Li–B–W–O/SUS/Si, an impedance measurement conducted at room temperature revealed an ionic conductivity of 2.15×10^{-7} S cm^{-1} with activation energy of 0.52 eV, which suggests that Li–B–W–O thin film can possibly be used as an electrolyte in solid-state thin film batteries.

S. H. Jee · J. Y. Oh · Y. S. Yoon (✉)
Department of Materials Science and Engineering, Yonsei University, 134 Shinchon Dong, Seoul 120-749, Korea
e-mail: yoonys@yonsei.ac.kr

H. S. Ahn · D.-J. Kim
Materials Research and Education Center, Department of Mechanical Engineering, Auburn University, 201 Ross Hall, Auburn, AL 36849-5341, USA

H. C. Wikle III
Razor Technologies Inc., 610 Jennifer Drive, Auburn, AL 36830, USA

S. H. Kim (✉)
GS Nanotech Inc., New Energy Development Center, 453-2 Seognae-dong, Gangdong-gu, Seoul 134-030, Korea
e-mail: shkim@gsnanotech.co.kr

Introduction

Since the 1970s, many solid-state electrolytes have been studied for use in solid-state ionic power devices, such as thin film microbatteries (TFBs) and thin film micro super capacitors (TFSCs) owing to their potential uses as main and alternative power sources in various applications [1–3]. Generally, either solid-state or liquid-state electrolytes may be found in energy storage devices. In comparison with the liquid-state electrolytes, solid-state electrolytes have not provided satisfactory performance to meet the requirements of practical field applications, where high ionic conductivity, chemical, and electrochemical stability are required [4]. However, solid-state electrolytes have a wider range of potential field applications in comparison with liquid-state electrolytes, due in part to the ease at which the fabrication of thin film forms of energy storage devices is possible. The solid-state electrolytes can be further divided into crystalline electrolytes and amorphous electrolytes. Amorphous electrolytes include a sulfide series and an oxide series. The sulfide series exhibit high ionic conductivity at room temperature and high thermal stability but they become unstable when they come into contact with moisture in the air. In addition, for all practical purposes, it is hard to use the sulfide series because they are quite difficult to handle. On the contrary, an oxide series solid-state electrolyte is chemically and electrochemically more stable than a sulfide series solid-state electrolyte at normal atmospheric conditions [4]. Therefore, an oxide solid-state electrolyte offers great potential for thin film-type electrolytes in TFBs and TFSCs.

The search for an excellent solid-state electrolyte with high ionic conductivity, as well as high thermal and chemical stability, is required to realize wide spread utilization of these ionic power devices. Most recent studies

have focused on the development of superior thin film electrodes to meet the challenges posed. The current status of solid-state electrolytes for these ionic power devices is still not sufficient, however. Many materials, such as the hydrogenated zirconia ($ZrO_2{\cdot}H_x$) [1], lithium lanthanum titanate (LLT) [5, 6], and lithium phosphorous oxynitride (LiPON) [7–9], have been used to deposit electrolyte thin films for solid-state ionic power devices. LiPON solid-state electrolyte thin films have been studied for TFBs and TFSCs because of their stability with Li metal, they are easily handled in normal atmospheric conditions and they exhibit relatively high ionic conductivity. It has been reported that the ionic conductivity of LiPON thin film grown as under various deposition conditions are in the range of 5×10^{-7}–2×10^{-6} S cm^{-1} at room temperature. However, the deposition time to obtain an optimal thickness of LiPON (about 1 μm) is too long for cost-effective application. Inaguma et al. [10–13] and Oguni et al. [14] have reported ionic conductivities of LLT thin film that were 10–100 times higher than that of LiPON thin films at room temperature. However, the as-grown LLT thin film showed several problems such as low growth rate and high deposition temperature when it was deposited directly onto the electrode. Based on our previous patent [15], Li–B–W–O can not only be evaporated by a thermal evaporation method but also forms a thicker film in a short time (about 5 min). In this study, we focused on the fabrication and characterization of lithium–boron–tungsten–oxide (Li–B–W–O) solid-state electrolyte thin films as a new solid-state electrolyte candidate for solid-state TFBs and TFSCs. To the best of our knowledge, no research has been reported on thermal evaporation grown Li–B–W–O thin films as a solid-state electrolyte.

Experimental

Li–B–W–O powders were synthesized from Li_2O, B_2O_3, and Li_2WO_4 (Kojundo Co. Ltd, 99.9%) as starting materials. Li_2O, B_2O_3, and Li_2WO_4 (Li_2O:B_2O_3:Li_2WO_4 = 2.7:1:1.2) were thoroughly mixed in a rotary mill for 48 h with ceramic balls using ethanol as the dispersing medium. The slurry was then dried for 24 h at a temperature of 100 °C. The obtained Li–B–W–O powder was calcinated at a temperature of 700 °C for 3 h. Following calcination, the powder was again dried for 24 h at a temperature of 100 °C and then ball-milled for 24 h. Finally, to obtain pellets of Li–B–W–O, the powder were pressed under a 100 kg cm^{-2} load. A final heat treatment at 700 °C was performed for 3 h to form the crystalline structure in the Li–B–W–O pellet. As shown in X-ray diffraction (XRD) spectrum of Fig. 1, a crystalline phase of the Li–B–W–O solid-state electrolyte pellet was observed.

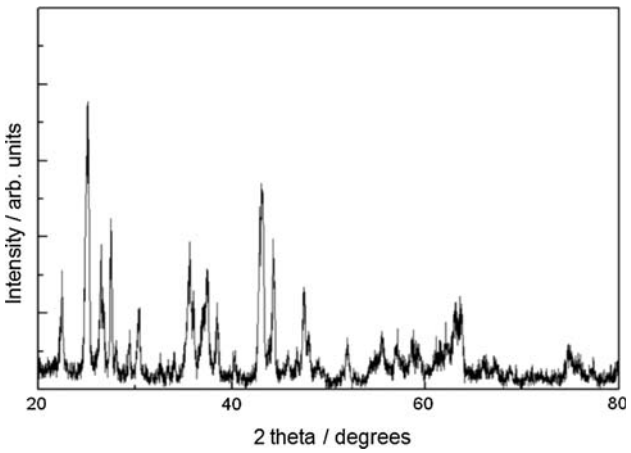

Fig. 1 XRD patterns of Li–B–W–O solid-state electrolyte pellet

Si substrates, which were degreased in acetone, methanol, and ethanol for 10 min, and then rinsed thoroughly using deionized water, were used in the thin film experiments. After preparing the substrates, a vacuum chamber was evacuated to 5×10^{-6} Torr. SUS (200 nm) bottom layers were deposited at room temperature by direct current (DC) sputtering using a 4-in. SUS metal target with a purity of 99.9%, where the Ar flow rate was maintained constant (21 sccm) at a working pressure of 5×10^{-3} Torr and an applied DC power of 40 W. Before deposition, the SUS metal target surface was pre-sputtered using an Ar^+ plasma to eliminate the oxide layer on the target surface. The pre-sputtering was performed for 10 min at a working pressure 5×10^{-2} Torr.

Li–B–W–O solid-state electrolyte thin films were grown on the SUS/Si substrate using a thermal evaporation deposition system with a base pressure of 5×10^{-6} Torr. The Li–B–W–O pellet was evaporated at a working pressure of 5×10^{-5} Torr with an input current of 2–2.5 A. After the Li–B–W–O thin film was deposited, an upper SUS electrode was grown by the same procedure as the bottom SUS electrode. These fabrication steps are schematically shown in Fig. 2. The final cell was a multilayered structure of SUS/Li–B–W–O/SUS/Si.

The chemical state and atomic composition of the as-grown Li–B–W–O solid-state electrolyte thin film was measured using X-ray photoelectron spectroscopy (XPS), inductively coupled plasma-atomic emission spectrometer (ICP-AES) (Li:B:W ratios), and energy dispersive X-ray spectroscopy (EDX). The binding energy scale was calibrated by assigning the C 1s signal at 284.6 ± 0.1 eV. For the crystal structure and phase analyses, XRD measurement with Cu Kα_1 radiation was performed. The cross-section and surface morphology observation of the SUS/Li–B–W–O/SUS/Si was carried out with field emission scanning electron microscopy (FESEM). Additionally, the ionic conductivities of the multilayered SUS/Li–B–W–O/

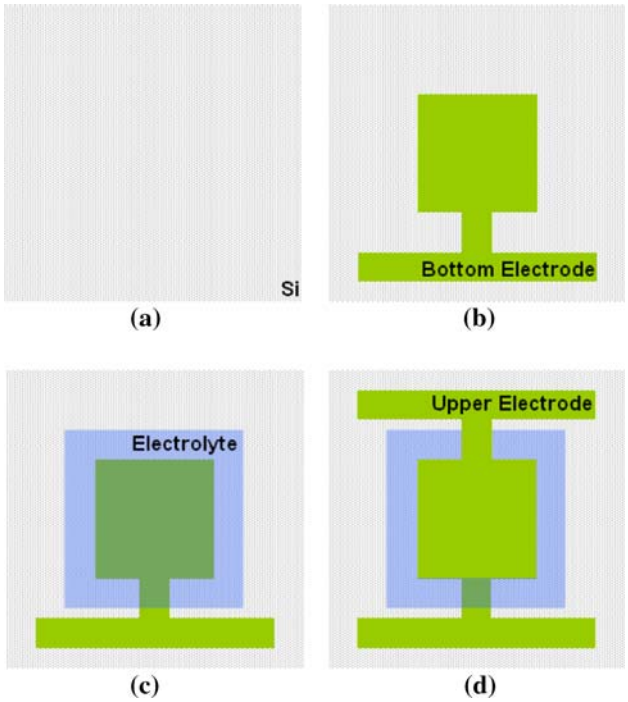

Fig. 2 Schematic illustration of cell fabrication processes

SUS/Si cell structures were measured by impedance analysis with the frequency range of 1 to 100 MHz at room temperature.

Results and discussion

The XPS O 1s peak of a Li–B–W–O solid-state electrolyte thin film on Si wafer is shown in Fig. 3. Curve fitting was performed with a mixed Gaussian (70%) and Lorentzian (30%) distribution, decomposed into three components. The full-width at half-maximum of the fitted curve is 1.85 ± 0.05 eV, which is in agreement with the binding energy reported by Leftheriotis et al. [16]. In metallic oxides, the binding energy of 530.5 eV is generally assigned to the bonding state of oxygen atoms and metal series (W=O) materials. Also, a second peak arises at the binding energy of approximately 531.9 eV. Leftheriotis et al. [17] reported that this peak has also been observed for evaporated WO_3 films and has been attributed to O atoms in substoichiometric WO_x structures. However, in our case, the XPS O 1s peak analysis of alkali borate glasses, rather than metal oxides series, applies because of the use of a boride series (B_2O_3) as a starting material. In alkali (lithium) borate glass materials ($LiBO_x$), the peak at 530.5 eV is due to the nonbridging oxygen, and the peak at 531.9 eV is attributed to the bridging oxygen species [18]. Therefore, the other O 1s peak observed at the 528.9 eV is attributed to lithium oxide (Li_2O series), which is due to chemical reaction when the lithium and oxygen ions combined during the thermal evaporation. Finally, a peak at 532.5 eV corresponding to oxygen in water molecules was not observed.

Figure 4 shows the evolution of the W 4f doublet peak of the Li–B–W–O solid-state electrolyte thin film. The measured binding energies of the doublet peaks are 33.9 and 36.2 eV for W $4f_{5/2}$ and W $4f_{7/2}$, respectively. The spin–orbit separation of the doublet peak was 2.3 eV, and the ratio of doublet peaks intensities was 0.78. Generally, the doublet peaks are classified at 35.6 eV for the W $4f_{5/2}$ and at 37.7 eV for the W $4f_{7/2}$. In comparison, the doublet W 4f peaks exhibited in our results shifted to a lower binding energy. The peak shift is caused by an increase in the number of nonbridging oxygen atoms present in the interface region, which agrees well with Hensley and Garofalini [18] and Tallan [19]. Also, we calculated the

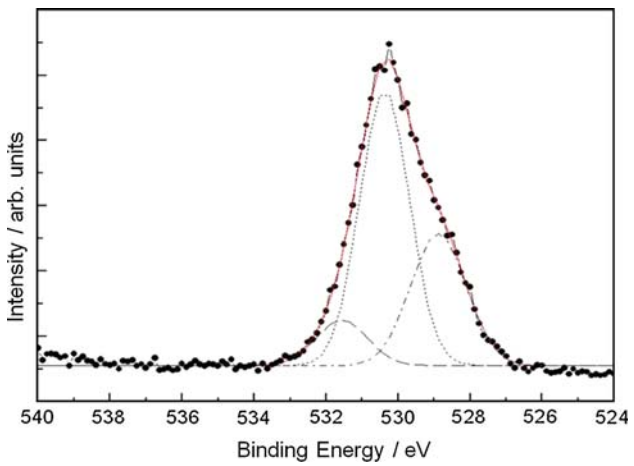

Fig. 3 XPS O 1s fitted spectrum of the as-grown Li–B–W–O solid-state electrolyte thin film

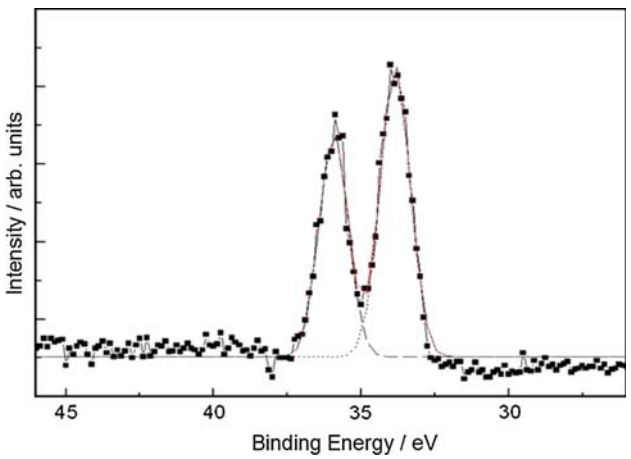

Fig. 4 XPS W 4f fitted spectrum of the as-grown Li–B–W–O solid-state electrolyte thin film

Table 1 ICP-AES analysis on the surface of the deposited of Li–B–W–O solid-state electrolyte thin film

	Compositional analysis (mol%)		
	Li	B	W
Electrolyte (Li–B–W–O)	5.9	1.97	0.09

Table 2 The molar ratio of each component for Li–B–W–O solid-state electrolyte thin film

	L	B	W	O
Electrolyte (Li–B–W–O)	2.99	1	1.8	9

O/W ratio by using the O 1s and W 4f XPS peak intensities, resulting in an O/W ratio of 5.0. This result is attributed to an excess of oxygen in the Li–B–W–O solid-state electrolyte thin film.

By comparing ICP-AES and EDX results, the final composition of the as-grown Li–B–W–O solid-state electrolyte thin film could be determined. Table 1 shows the ICP-AES results. Based on ICP-AES and EDX data, the molar ratios of Li–B–W–O thin film was shown in Table 2. The Li/B composition ratio of Li–B–W–O solid-state electrolyte thin film result was 2.99. Consequently, the composition of as-grown Li–B–W–O solid-state electrolyte thin film is $Li_{2.99}BW_{1.8}O_9$.

No indication of defects such as cracks, grooves, pinholes, or pores was observed in the as-grown Li–B–W–O solid-state electrolyte thin film, as confirmed by visible inspection and optical microscopy. Figure 5a shows the FESEM cross-section images of the SUS/Li–B–W–O/SUS/Si cell. This image shows that the thicknesses of the bottom electrode and electrolyte layer were 0.08–0.14 and 1.16 μm, respectively. In addition, there was no indication of interfacial diffusion between the electrode and electrolyte layer. The FESEM image of the bottom electrode–solid-state electrolyte–upper electrode sandwich structure confirmed that it possessed a high-density structure without any defects such as cracks or voids. Also, no columnar structure was found in the as-grown solid-state electrolyte thin film. In general, the grain boundary formed by a columnar structure has a large potential for electron transport or short circuiting. In the FESEM micrograph of Fig. 5b, the as-grown Li–B–W–O solid-state electrolyte thin film, however, exhibits amorphous-like surface characteristics. This morphology reflects the typical surface structure of an amorphous thin film such as the absence of grains and grain boundaries. An amorphous structure was confirmed by XRD spectrum analysis of the as-grown Li–B–W–O solid-state electrolyte thin film. As shown in Fig. 6, no crystalline phase was observed in the XRD spectrum of the Li–B–W–O thin film. In all solid-state

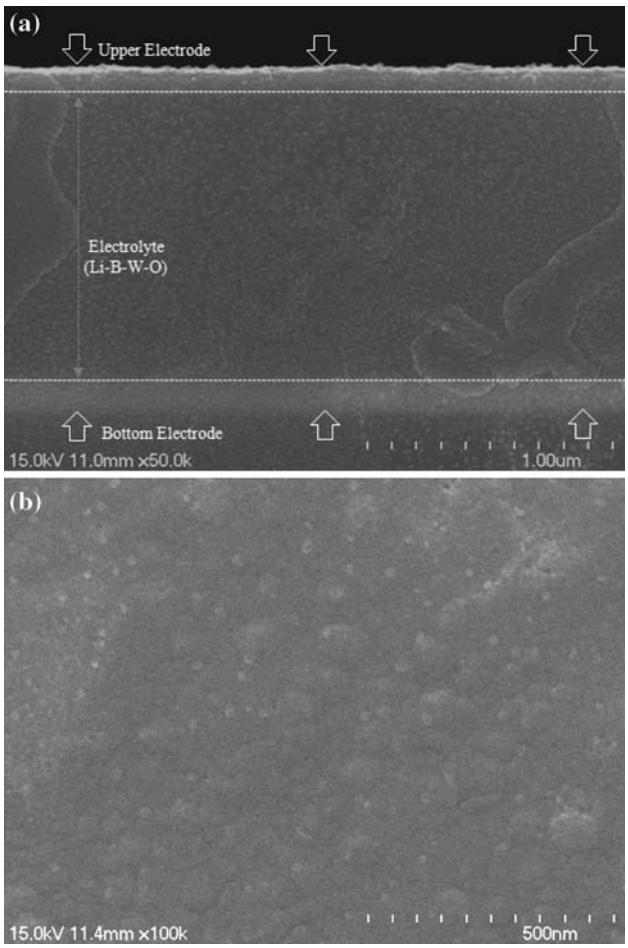

Fig. 5 The FESEM (**a**) cross-section of cell structure and (**b**) surface morphology images of Li–B–W–O solid-state electrolyte thin film

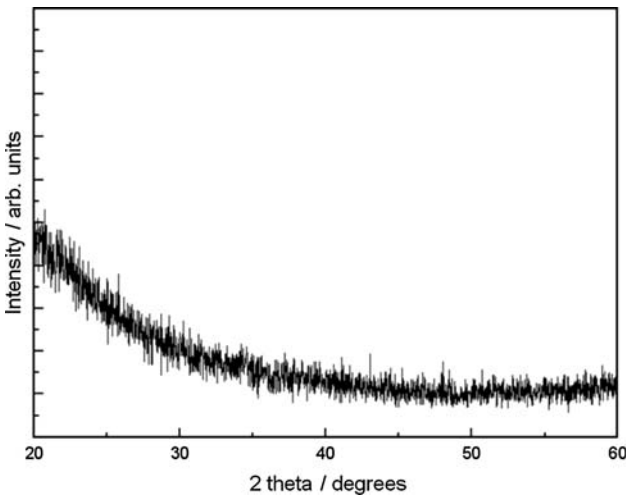

Fig. 6 XRD patterns of Li–B–W–O solid-state electrolyte thin films as grown by thermal evaporation deposition method

ionic power devices, the surface structural properties are very important because the presence of these types of defects can act as an electronic current path or leakage

source [20]. Therefore, it is critical for a deposition of the Li–B–W–O solid-state electrolyte thin film to be without defects and to possess a very smooth surface to prevent the possibility of short circuits occurring in solid-state ionic power devices.

Figure 7 shows the impedance spectrum of the SUS/Li–B–W–O/SUS/Si cell structure at room temperature. In the case of the as-grown Li–B–W–O solid-state electrolyte thin film, only one semicircle was observed corresponding to a bulk conduction mechanism since there are no grain boundaries present in the amorphous Li–B–W–O thin film. The ionic conductivity was calculated by means of the following equation:

$$\sigma = d/R \times A \quad (1)$$

where d is the thickness of solid-state electrolyte, R is the electrolyte resistance, and A is the electrode area. The Li–B–W–O solid-state electrolyte thin film exhibited an ionic conductivity of 2.15×10^{-7} S cm^{-1} which is similar to other reported values [7–9].

Activation energy (E_a) for Li–B-W–O thin film solid-state electrolyte was calculated by the following equation, using the Arrhenius equation and measured conductivity at various temperatures.

$$\sigma T = (\sigma T)_0 \exp(-E_a/kT) \quad (2)$$

where σ is the ionic conductivity, k is the Boltzmann constant, and T is the temperature. The activation energy of Li–B–W–O solid-state electrolyte (0.52 eV) was smaller than that of LiPON (0.55 eV) in the previously reported work [21]. These results suggest that Li–B–W–O thin films could possibly be used for electrolytes in solid-state ionic power devices (Fig. 8).

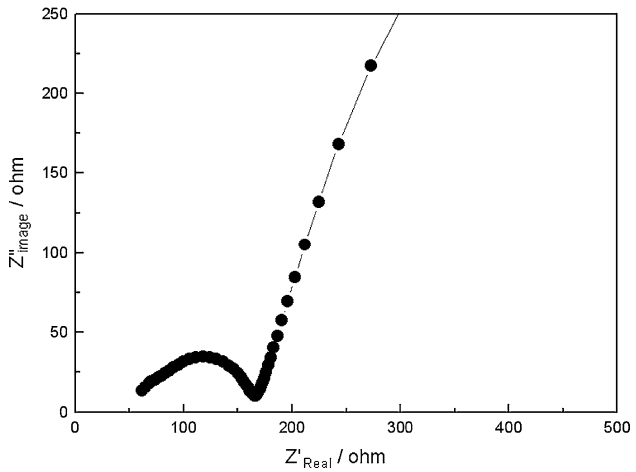

Fig. 7 Impedance diagram of Li–B–W–O solid-state electrolyte thin film at room temperature

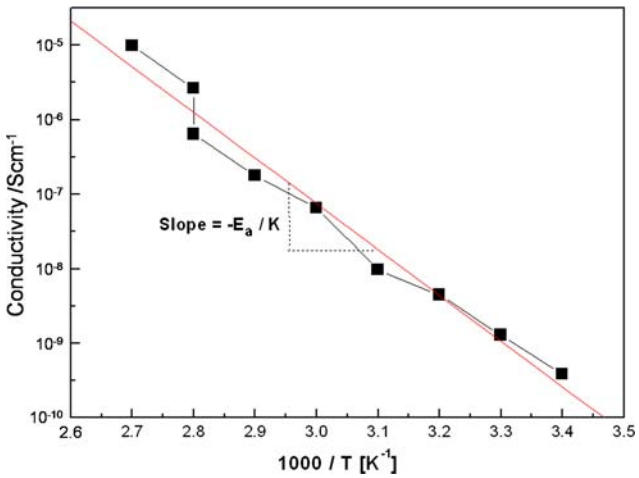

Fig. 8 Arrhenius plot for ionic conductivity of Li–B–W–O solid-state electrolyte thin film as a function of temperature

Conclusions

The fabrication and characterization of Li–B–W–O solid-state electrolyte thin films as grown by a thermal evaporation deposition method were investigated to develop a new candidate solid-state electrolyte for ionic power sources. The structural properties of the as-grown Li–B–W–O solid-state electrolyte thin film have been investigated using XRD, FESEM, and XPS. The as-grown film exhibited a peak shift to lower binding energies for the O 1s and W 4f peaks due to the excess of the oxygen.

As revealed by the EDX and ICP-AES measurements, the stoichiometry of the as-deposited Li–B–W–O solid-state electrolyte thin film was $Li_{2.99}BW_{1.8}O_9$. A room-temperature ionic conductivity of 2.15×10^{-7} S cm^{-1} was obtained with the multilayered cell structure of SUS/Li–B–W–O/SUS/Si, suggesting that a Li–B–W–O thin film can possibly be used as an electrolyte in solid-state ionic power devices.

Acknowledgement This work was supported by Priority (NRF) funded by the Ministry of Research Centers Program through the National Research Foundation of Korea Education, Science and Technology (2009-0093823).

References

1. Kim SH, Ko JH, Ji SH, Kim JS, Kang SS, Lee MJ, Yoon YS (2006) Jpn J Appl Phys 45:5144
2. Liu HK, Wang GX, Guo Z, Wang J, Konstantinov K (2006) J Nanosci Nanotechnol 6:1
3. Nagasubramanian G, Doughty DH (2004) J Power Sources 136:395
4. Lee S, Kim J, Shin D (2007) Solid State Ionics 178:375
5. Chen CH, Amine K (2001) Solid State Ionics 144:51
6. Bohnke O, Bohnke C, Fourquet JL (1996) Solid State Ionics 91:21

7. Jeong EY, Hong C, Nam SC, Cho SB, Tag YS (2006) J Power Sources 159:223
8. Kim BS, Cho YS, Lee J-G, Joo K-H, Jung K-O, Oh JM, Sohn H-J, Kang T, Cho JP, Park Y-S, Oh JY, Park BW (2002) J Power Sources 109:214
9. Choi CH, Cho WI, Cho BW, Kim HS, Yoon YS, Tak YS (2002) Electrochem Solid-State Lett 5:A14
10. Inaguma Y, Chen L, Itoh M, Nakamura T, Uchida T, Ikuta H, Wakihara M (1993) Solid State Commun 86:689
11. Inaguma Y, Chen L, Itoh M, Nakamura T (1994) Solid State Ionics 70–71:196
12. Inaguma Y, Okuyama N, Atsumi Y, Katsumata T (2002) Chem Lett 1106–1107:11
13. Inaguma Y, Chen L, Itoh M, Nakamura T (1995) J Electrochem Soc 142:L8
14. Oguni M, Inaguma Y, Itoh M, Nakamura T (1994) Solid State Commun 91:627
15. Choi J-W, Yoon YS, Kim SH, Ko JH, Korean Patent Appl. No. 10-2007-0128818, 12 Dec 2007
16. Leftheriostis G, Papaefthimiou S, Yianoulis P, Siokou A, Kefals D (2003) Appl Surf Sci 218:276
17. Leftheriostis G, Papaefthimiou S, Yianoulis P, Siokou A (2001) Thin Solid Films 384:298
18. Hensley DA, Garofalini SH (1994) Appl Surf Sci 81:331
19. Tallan NM (ed) (1974) Electrical conductivity in ceramics and glass, part B. Marcel Dekker, New York, pp 559–618
20. Lee J, Kim SH, Tak Y, Yoon YS (2006) J Power Sources 163:173
21. Bate JB, Dudney NJ, Gruzalzki GR, Zuhr RA, Choudhury A, Luck CF, Robertson JD (1992) Solid State Ionics 53–56:647